Sr immobilization in irradiated Portland cement paste exposed to carbonation

Gabriela Bar-Nes, Ofra Klein-Bendavid, Laure Chomat, Nathalie Macé, Michal Arbel-Haddad, Stéphane Poyet

Sr immobilization in irradiated Portland cement paste exposed to carbonation

Gabriela Bar-Nes[1]*, Ofra Klein-BenDavid[1], Laure Chomat[2], Nathalie Macé[2], Michal Arbel-Haddad[1], Stephane Poyet[2]

[1] Department of Applied Chemistry, NRCN, P.O. Box 9001, Beer-Sheva, Israel.

[2] Den-Service d'Etude du Comportement des Radionucléides (SECR), CEA, Université Paris-Saclay, F-91191, Gif-sur-Yvette, France

*Corresponding author: gabi.barnes@gmail.com

Abstract

Cement based materials are widely used as binding matrices for radionuclides in low and intermediate level waste management applications. We studied the effect of irradiation and carbonation under atmospheric condition on the leaching of Sr from Portland cement paste. Samples were exposed to gamma irradiation or subjected to thermal treatment under either inert or atmospheric conditions. Leaching tests were performed and supplemented by post-leaching characterization including local chemical analysis (LA-ICPMS) crystallographic analysis (XRD), and EPMA imaging. The combination of these methods enabled us to link between the crystallography, texture and composition of the treated samples and their ability to retain Sr ions. Results show that carbonation was the main factor determining the retention of Sr ions, whereas irradiation did not have a significant effect. Moreover, carbonation has a positive effect on the retention of Sr ions in the matrix with the formation of a carbonated zone.

Keywords:

cement paste (D), carbonation (C), radioactive waste (E), leaching, characterization (B)

1. Introduction

Cement based materials are widely used in the nuclear industry for low and intermediate level waste management applications due to their availability, low cost, good chemical compatibility with waste ions and mechanical stability. The prediction of the long-term behavior of cementitious waste packages requires the identification and the understanding of degradation mechanisms that might affect the structure. One of these degradation mechanisms is water radiolysis, resulting from the immobilized radioactive waste elements, which leads to dehydration and release of H_2 gas, and thus carries potential impacts on the safety of the wasteform [1,2]. Cement carbonation occurring at atmospheric conditions (in presence of CO_2), is an additional degradation mechanism that could affect the waste-form stability [2,3]. The temperature increase induced by the irradiation could produce favorable conditions for enhanced carbonation. The extent of carbonation depends on CO_2 partial pressure [4-6], moisture content in the sample pores [4,7-9] and temperature [10-12]. Although the carbonation reaction occurs in the aqueous phase and therefore slows down as water activity decreases, at highly saturated conditions the diffusion of carbon dioxide is reduced and even inhibited by water filling the pores. Therefore, carbonation occurs most rapidly at intermediate saturation of the cement paste.

There are few published data on the effect of irradiation on the immobilization of radioactive waste in cement based materials. One of the studies [2] concluded that the enhanced carbonation associated with irradiation, leads to crystallographic, textural and chemical modifications and thus affects the immobilization of radionuclides in the matrix. The effect of carbonation on the leaching resistance of cementitious pastes has been extensively studied [13-16], but contradictory results were reported. These contradictions originate from the fact that in some cases carbonation might improve waste retention either by precipitation as insoluble carbonates, or due to the reduced

porosity of the carbonated matrix, while in other cases retention was reduced, possibly as a result of micro-cracking due to shrinkage during carbonation or rearrangement in pore connectivity [15-19].

The objective of this study is to gain understanding concerning the combined effect of irradiation and carbonation on Sr retention in cement paste. The experimental approach included the exposure of cement samples to different degradation mechanisms (irradiation and thermal treatment under either inert or atmospheric conditions) followed by leaching tests. The samples were studied using XRD, to obtain their crystalline phase composition before and after treatment and leaching. LA-ICP-MS and EPMA were applied to explore the local changes in the chemical composition due to the various treatments, allowing the evaluation of the different treatments on the durability and leaching resistivity of cementitious pastes.

2. Experimental

2.1. Sample preparation

The cement used for this study is a CEM I Val d'Azergues cement from Lafarge Company (France). It is composed of 96% of clinker, 1% of filler and 3% of gypsum. The chemical composition of the cement is presented in Table 1. Cementitious samples were prepared with a water to cement ratio (w/c) of 0.4. A non-radioactive Sr solution, using the nitrate salt, $Sr(NO_3)_2$ (Aldrich chemicals), has been added to the cement to prepare a Sr-spiked-cementitious paste, in order to simulate a waste stream to be cemented, with a target Sr concentration of 3.66 mg Sr/g paste. Non-spiked (blank) samples were prepared in order to assess the effect of the Sr addition on the on the crystallography, texture and composition of the paste.

All specimens were cast in plastic molds (diameter of 40 mm and height of 100 mm) and sealed. After setting, the samples were de-molded, inserted into polypropylene bags, sealed again and allowed to self-cure at room temperature for 28 days. The cured specimens were sliced using a diamond saw into 15 mm thick disc shaped samples. The list of samples is presented in Table 2.

2.2 Degradation procedures

2.2.1 Gamma irradiation

Sample irradiation was performed using a ^{60}Co source in a commercial irradiation facility (Sorvan Ltd, Israel). The irradiation has been performed at a dose rate of 24 Gy/min, over a period of 6 months, to reach a total dose of $5.0x10^6$ Gy.

Samples were irradiated either under inert conditions or exposed to the ambient atmospheric conditions of the irradiation cell. Samples irradiated under inert conditions were placed in Pyrex® ampoules and sealed at sub-atmospheric pressure (500 torr) and under an Ar atmosphere. As the irradiation cell lacks climate control, fluctuations in the atmospheric conditions are expected during the irradiation period. The average operating temperature and the relative humidity in the irradiation chamber were ~40°C and ~30%, respectively.

2.2.2 Thermal degradation

Samples exposed to thermal degradation were polished before the treatment in order to remove any possible surface alteration prior to the experiment.

89 Samples were placed inside a climatic chamber at 40°C, 32% RH at atmospheric conditions for 6
90 months. Samples treated under inert conditions were placed in a reactor filled with N_2 at 32% RH,
91 fixed by a $MgCl_2$ saturated solution [20], inside the same climatic chamber.

92 2.3 Characterization methods

93 2.3.1 XRD analysis

94

95 Crystallographic characterization was performed using X-Ray diffraction (XRD). Measurements
96 were carried out using a PANalytical X'Pert diffractometer (Cu Kα, λ = 1.54 Å), on the angular
97 range of 5° - 65°, in increments of 0.017° or 0.033°.

98 XRD analyses were performed on bulk samples. Analysis of bulk samples eliminates a preliminary
99 grinding and avoids possible effects of preferential orientation encountered in the powder method.

100 In order to obtain XRD profiles, the polished surface was analyzed, consequently a thin layer of
101 the sample (from 30 to 150 μm of thickness) was removed by polishing and the newly exposed
102 surface was then analyzed. This method allowed us to obtain a series of diffractograms as a
103 function of the depth of the sample. Prior to the XRD characterization, five points were marked on
104 the bottom of the sample and the sample thickness at each of the points was measured using a
105 micrometer screw gauge. The samples were then manually polished using 120 grit silicon carbide
106 paper. After each polishing step, the sample thickness was measured again at each of the 5 points
107 using the micrometer screw gauge. For each of the 5 measured points the difference between the
108 initial thickness and the measured thickness (which refers to the measured depth) was calculated.
109 The average of all 5 points was denoted as the sample depth analysed. Grinding was preformed up

110 to a depth of approximately 3500 μm in the sample, until reaching the non-altered part of the
111 sample.

112 XRD results were analyzed using the Reference Intensity Ratio (RIR) method [21](Johnson and
113 Zhou, 2000) which scales all diffraction data to a Corundum (Al_2O_3) standard. The RIR factors
114 were obtained from ICSD using POWD-12++ and are presented in Table 3. The scale factors are
115 determined from the strongest intensity lines of both the analyte and corundum. In cases where the
116 calculation was performed using a different diffraction line, an additional correction factor was
117 applied, proportional to the relative intensity of the chosen diffraction line as compared to the
118 strongest diffraction line, denoted here as peak fraction.

119 Due to the presence of non-crystalline phases in the cementitious matrix, the RIR approach was
120 used as a semi-quantitative method, allowing us to normalize the diffraction intensities, and thus
121 making qualitative comparison only between the different crystalline phases in a specific sample.
122 Therefore the results are presented as intensity normalized by RIR factor and the peak fraction
123 (Table 3).

124 2.3.2 LA-ICPMS analysis

125 Cement samples were cleaved, exposing a cross-section extending from the surface into the sample
126 core. Each sample was placed in a cell equipped with an inlet nozzle of 0.5 mm diameter. Laser
127 ablation was conducted using an ArF-excimer laser (New Wave) emitting 15 ns long pulses at a
128 wavelength of 193 nm, with repetition rate of 10 Hz, at a power of 7 J/cm^2 , with fluence of 5.05
129 J/cm^2. The cell was flushed with 0.5 L/min helium, washing the vaporized sample into the mass
130 spectrometer. SRM NIST610 glass was used as standard. Ablation of the standard was conducted
131 at the beginning and the end of each ablation session, at a spot size of 50 μm.

The analyzed spot size varied across the cement samples in order to attain maximal resolution near the surface where leaching and precipitation are expected to have the strongest effect, and a lower resolution but higher signal at inner sample areas. A spot size of 10 μm was used at the outermost 120 μm of the sample, then a spot size of 50 μm was applied for the next 900 μm, and finally a spot size of 100 μm was used for the innermost 3000-4000 μm.

The ICP-MS analysis was conducted by AGILENT (7500 CX) ORS quadrupole mass spectrometer with a RF power of 1500W, injection tube diameter of 2.0 mm, nebulizer and auxiliary gas flows of 0.9 L/min Ar .

Table 4 lists the analyzed isotopes, the average limit of detection for the different isotopes at different spot sizes and the average analytical error for the various isotopes as a function of the spot size used.

For all three spot sizes the average error is generally lower than 3% (except for Ba in the 10 μm spot size) An average error lower than 1% is obtained for all isotopes at 100 μm spot size. For ^{88}Sr and ^{42}Ca, the most important analytes in this paper, the analytical error is ≤1%.

SiO_2 was used as an internal standard, at a concentration of 20.6% (the concentration measured in the original cement powder).

SiO_2 was used as its concentration is relatively high, thus, it is easily detected using the ICP-MS. Furthermore, Si concentration is not expected to decrease significantly due to leaching effects.

In order to obtain coherent concentration display between all the samples, the different element concentrations (C) are presented relative to the concentration of the innermost spot analyzed (C0), assuming that this point resides within the undisturbed inner sample volume.

Figure 1 shows the normalized ^{25}Mg and ^{42}Ca signals obtained as a function of distance from the surface of a leached sample, together with the analyzed spot size used. These results demonstrate

155 that in spite of the higher limit of detection and larger error for the smaller spot size, spot size has
156 no effect on the calculated concentration of Mg, representing an element with minimal leaching.
157 Additionally, no correlation was found between the spot size used and the concentration calculated
158 for Ca, confirming that concentration changes are not an artifact of the spot size.
159
160 2.3.3. EPMA (Electron Probe Micro-Analysis)
161
162 Samples were impregnated in epoxy (Epofix by Struers) using a Citovac device (by Struers) for
163 10 min at a pressure of 0.73 bar. The impregnated samples were polished parallel to the sample
164 surface using a Saphir 250 polishing machine manufactured by ATM. The samples were initially
165 polished using SiC polishing paper with 320, 600 and 1200 grid, and finally using a diamond
166 suspension of 3 and 1 μm. Samples were then carbon coated and mounted on the EPMA stand.
167 EPMA imaging and analyses were conducted using a JEOL 8230 superprobe EPMA with EDS
168 (Energy-Dispersive X-ray Spectroscopy) and four wavelength-dispersive spectrometers (WDS)
169 for microanalysis. Beam conditions were set to 15 keV and 15 nA. Silicate and oxide standards
170 were used for EDS analyses. Data was processed with a PRZ correction procedure. Back-scattered
171 electron (BSE) and secondary (SEC) electron imaging were applied.

172 2.4 Leaching experiments

173 The leaching tests were performed according to the standard ANS-16.1 procedure [22], using
174 deionized water as the leachant. According to this procedure, the leachant volume (cm^3) equals 10
175 times the surface area of the tested sample (cm^2). Samples were immersed for 90 days, with
176 leachant replacement at predetermined leaching intervals of 2, 7, 24, 48, 72, 96, 120, 456, 1128,

177 and 2136 hours. Following the standard procedure, the leaching tests were performed in closed
178 vessels under static, atmospheric conditions.

179 Leaching tests have been performed for samples treated under the different conditions and for
180 untreated reference samples. Duplicate samples containing Sr were tested except for the sample
181 irradiated at inert conditions, for which a single sample was available.

182 To assess the effect of initial Sr concentration on the leachability, an additional blank sample
183 prepared with no Sr doping was tested.

184 The concentrations of Sr and Ca in the leachate were determined using Inductive Coupled Plasma
185 Optical Emission Spectroscopy (SPECTRO ARCOS ICP-OES) for each leaching interval.

186 ## 3. Results

187 ### 3.1 Crystallographic characterization of untreated HPC (hydrated Portland cement) samples

188 The powder diffraction pattern of a crushed non-treated sample (not presented) displays the typical
189 crystallographic composition for a CEM I cementitious paste: portlandite ($Ca(OH)_2$), ettringite
190 ($Ca_6Al_2(SO_4)_3(OH)_{12}.26H_2O$) and C-S-H (calcium silicate hydrate phases) as hydrated phases and
191 possible presence of a small amount of calcite ($CaCO_3$) and some residual anhydrous phases (C_4AF
192 for $(CaO)_4Al_2O_3Fe_2O_3$, C_2S for $(CaO)_2SiO_2$ and C_3S for $(CaO)_3SiO_2$). As expected, no Sr bearing
193 phases have been identified by XRD analysis.

194 3.2 Characterization of treated HPC samples

195 3.2.1 Characterization of samples aged under inert conditions

196 Surface XRD analysis of samples treated under inert conditions (not presented) showed the full
197 disappearance of ettringite. Additionally, in the irradiated samples calcite was detected at the
198 surface, with a corresponding depletion of portlandite. This superficial precipitation had probably
199 occurred during sample preparation. Calcite was not found at the surface of the sample treated in
200 the climatic chamber which was polished prior to the thermal treatment (section 2.2.2).

201 EPMA imaging of a sample irradiated under inert conditions and the corresponding relative
202 concentrations of Ca, Ba and Sr as obtained by LA-ICPMS are presented in Figures 2 and 3,
203 respectively. The EPMA BSE image of the sample shows a very thin uneven front (10-100 μm) at
204 the sample surface, with a denser but brighter appearance (Fig. 2), while the rest of the sample
205 remains virtually unchanged.
206 The concentration profiles of Sr, Ca, and Ba along a cross-section in the same sample (Fig. 3)
207 indicate a constant concentration for these three elements throughout most of the sample, except
208 for the 80-100 μm outer surface, where the concentration of all three elements shows significant
209 scatter. This scatter might reflect the uneven precipitation of a carbonate phases near the surface.
210 The precipitation of such phases is probably due to exposure to atmospheric conditions during
211 sample preparation. These results are in agreement with the formation of a thin calcite layer at the
212 sample surface as observed by XRD, and with the EPMA-BSE image showing a thin dense layer
213 at the sample surface.
214

215 3.2.2 Characterization of samples treated under atmospheric conditions

Samples aged under atmospheric conditions, either in the climatic chamber or during the irradiation process, present similar crystallographic patterns.

The crystallographic composition of both samples consists of calcite near the surface of the sample with corresponding disappearance of the portlandite. Further into the sample aragonite and vaterite, the two metastable calcium carbonate phases, occur. The formation and stability of these two phases are favored over calcite at temperatures above 40°C [23,24]. The overall thickness of the carbonated zone, defined by the presence of calcium carbonate phases, is about 3500 μm, for both irradiated and non-irradiated samples (Fig. 4).

Samples treated in the climatic chamber exhibited cracking after three days of treatment (Fig. 5), probably due to the enhanced drying process.

3.3 Leaching results

Leaching experiments were performed for samples exposed to various aging treatments as well as for untreated reference samples. Figures 6 and 7 present the average cumulative fraction of Sr and Ca ions leached for the different samples *vs*. square root of time.

The overall cumulative fraction values obtained for Sr were higher than for Ca, although the trends were similar. For the reference sample, for example, the cumulative fraction of Sr was five times higher than for Ca (0.09 and 0.018 respectively).

For samples aged under atmospheric conditions, and hence exposed to carbonation, the cumulative fraction of both Sr and Ca ions leached was lower than for untreated reference samples, with no apparent difference between the irradiated and climatic chamber samples.

The sample that has been exposed to irradiation under inert atmosphere showed a slight increase in the cumulative Sr and Ca leached fraction compared with the reference sample. Significant increase in the leached fraction of Sr and Ca was obtained for the samples that were treated in the climatic chamber under inert atmosphere. For these samples the Sr and Ca cumulative fractions increased from values of 0.09 and 0.018 in the reference sample, to values of 0.35 and 0.044; respectively.

The difference between the results obtained for irradiated and climatic chamber samples treated under inert atmosphere could be a result of differences in the sample pre-treatment. As presented in section 3.2.1, the irradiated sample showed a thin carbonation zone. Such carbonation zone was not found for the samples treated in the climatic chamber, which were polished before treatment.

The effect of initial Sr concentration on the Sr retention can be studied from the leaching curves of the two samples irradiated under inert conditions (Fig. 8), one doped with Sr and the other containing the native Sr content from CEM I cement (3660 ppm *vs.* 250 ppm respectively). Despite the large difference in the initial Sr concentration the cumulative leached fractions obtained were almost similar. Similar leachabilities were observed for both samples during the early stages of leaching, while a slightly higher leached fraction for the sample doped with Sr was measured at the later stages of the experiment.

3.4 Post leaching characterization

The distribution of the alkaline earth elements Sr, Ba and Ca within the leached samples, as obtained from LA-ICP-MS, will be presented together with the phase distribution as obtained from XRD depth profile measurements and complemented with EPMA images. Sr was considered as waste simulant, while Ca is a major cement component and Ba is a trace element present in cement.

Both Sr and Ba may substitute Ca in various mineral phases (especially carbonates) with high compatibility [25].

3.4.1 Post-leaching characterization of untreated reference sample

The untreated sample that served as a reference for the leaching test was analyzed after leaching. Figure 9 presents the EPMA BSE image of the sample. A very distinct disturbed zone can be detected at the surface. This zone, which is composed of several sub-zones, has an overall thickness of 700 μm.

The Sr, Ca and Ba relative concentration profiles along this reference sample are presented in Figure 10. All three elements show a decrease in relative concentration moving from the inner undisturbed zone (C/C_0= 1) towards the surface of the sample.

For all three elements, the concentration is relatively constant along the outer 700 μm, except for the outermost ~150 μm, where a large dispersion of the concentrations was found. This region roughly corresponds to the disturbed zone in figure 9. Further into the sample a relatively constant increase in the Sr concentration, with no corresponding morphological changes in the BSE image, is obtained until ~1600 μm, where the concentration levels to C/C_0 = 0.8. A further increase in the C/C_0 is observed at ~3000 μm reaching the level of C/C_0 = 1 at ~4000 μm. For both Ca and Ba the concentration reaches the level of C/C_0 = 1 at ~1000 μm.

Figure 11 presents the XRD profile of the same sample. At the surface, a carbonated zone is detected, indicated by the presence of calcite together with a reduction in the portlandite intensity. The normalized intensity for calcite is relatively high for the first 300 μm from the surface of the sample and then is gradually decreases up to a depth of approximately 800 μm into the sample, roughly corresponding to the disturbed depth as observed by EPMA (Fig. 9) and to the constant concentrations of all three elements studied (Fig. 10).

281 3.4.2 Post-leaching characterization of samples aged under inert conditions

282 Figure 12 presents an EPMA BSE image of the sample treated in the climatic chamber under inert
283 conditions. The image presents a highly porous, irregular dark area at the sample surface and along
284 two deep cracks which are perpendicular to the surface. These cracks seem to be inter-connected
285 and penetrate approximately 1000 μm into the sample. The bulk of the sample contains a brighter,
286 denser looking material.
287 Figure 13 presents the element concentrations along a cross-section of the samples aged under
288 inert conditions. Both samples show relatively large scatter of all three elements within the 100
289 μm nearest to the surface, followed by a relatively constant concentration of all three elements up
290 to a depth of 500-700 μm.
291 Further into the sample, the Sr concentration gradually increases until reaching values similar to
292 those of the undisturbed region (C/C_0= 1) at a depth of about 3000 μm for the irradiated sample
293 and 3800 μm for the sample treated in the climatic chamber. The Ca and Ba concentration profiles
294 show a step-like increase at a depth of 700 μm, reaching a constant value of ~ C/C_0= 1.
295 XRD measurements of the above samples reveal the depletion of portlandite from the outermost
296 region. Portlandite is detected at a depth of approximately 500-700 μm from the surface, in
297 accordance with the Ca concentration profile. Both samples show the presence of calcite at the
298 sample surface, gradually decreasing to a depth of approximately 500-700 μm (Fig. 14). Higher
299 intensity values of calcite were measured for the irradiated sample, in accordance with the higher
300 scatter at the surface probably due to an initial carbonation layer present in the sample, as
301 previously discussed in sections 3.2.1 and 3.3.

302 3.4.3 Post-leaching characterization of samples treated under atmospheric conditions

303 Figure 15 presents an EPMA BSE image of the sample treated in the climatic chamber under
304 atmospheric conditions. A thin (50-80 μm) porous rim is observed at the outer surface of the
305 sample. Porous regions are also observed along cracks which are perpendicular to the surface and
306 penetrate up to 300 μm. Beyond this porous rim, a zone of denser and brighter material, having a
307 thickness of 200 μm, is observed. The inner part of the sample keeps a relatively uniform
308 appearance.
309 Figure 16 presents the Ca, Sr and Ba relative concentration cross section along two samples
310 exposed to atmospheric conditions, either irradiated or treated in the climatic chamber. Both
311 samples show significant scatter near the surface. For the sample treated in the climatic chamber,
312 all three elements are depleted in the outermost 100 μm. For the irradiated sample Sr and Ba are
313 enriched in the outermost 100 μm. The concentration of all three elements was found to increase
314 from a depth of ~100 to ~1000 μm. The Ca concentration reaches its undisturbed concentration
315 (C/C_0~1) at ~1000 μm into the sample. For Sr and Ba, however, enrichment relative to the initial
316 concentration (C/C_0>1) is observed at a depth range of 700-4000 μm, with a gradual decrease back
317 to the undisturbed value.
318 Figure 17 presents the XRD measurements of the above samples. In both cases portlandite is
319 depleted from the surface up to a depth of 250-300 μm. From this depth inward there is a gradual
320 increase in portlandite to its maximal intensity.

321 Calcite was found at the surface of both samples. Its intensity decreases towards the inner part of
322 the sample and levels off at around 300 μm depth. The vaterite and aragonite phases are present
323 up to 3500 μm from the surface. The intensity curves slightly differ between the two samples.
324 While for the sample treated in the climatic chamber maximal intensity for both phases was
325 detected at around 50-100 μm from the surface, for the irradiated sample both carbonate phases

were not detected at the surface and appeared at a depth of 100 μm with a maximal intensity around 150 μm. For both samples the normalized intensity of vaterite was higher than that of aragonite.

4. Discussion

4.1 Leaching effect – samples treated under inert conditions

The post-leaching reactive concentration profiles obtained for samples aged under inert atmosphere, present an extended disturbed profile for all three examined elements, as compared to the reference sample. This corresponds well with the higher cumulative leached fraction obtained for these samples, possibly due to the formation of microcracks, which is known to occur during the enhanced drying process.

When comparing the two samples treated under inert conditions, it can be seen that the sample treated in the climatic chamber shows much higher leachability and deeper depletion profile relative to the sample exposed to irradiation.

As already discussed in section 3.2.1, the major difference between these two samples was the very thin carbonated layer present in the irradiated sample which was prior to treatment removed by polishing from the sample placed in the climatic chamber. This carbonated layer, a few tens of micrometers thick, may contribute to the reduced leachability of the sample irradiated under inert atmosphere.

An additional reason for the difference between the two samples could be the increased dehydration and consequent cracking due to the lower RH conditions (32%) fixed in the climatic chamber, compared to the irradiated sample sealed in an ampoule and thus exposed to much higher relative humidity (>80%).

347 The cumulative leaching fractions of samples with different initial Sr concentration (3660 ppm *vs.*
348 250 ppm Sr) were almost similar. A slightly higher leached fraction for the sample doped with Sr,
349 may result from a higher fraction of Sr residing in the interstitial pores for the doped sample
350 relative to the non-doped one, where a higher fraction of Sr is probably bound within the lattice
351 sites.

352

353 4.2 Leaching effect – samples treated under atmospheric conditions

354 In the present study samples were exposed to carbonation at 40°C either in a climatic chamber or
355 during the irradiation process. Both samples exhibit a ~3500 μm thick carbonated layer, composed
356 mainly of metastable calcium carbonate phases (vaterite and aragonite). The dominance of vaterite
357 and aragonite in the carbonated layer is in agreement with previous studies showing that hexagonal
358 vaterite precipitation predominates at 40°C, a temperature at which orthorhombic aragonite starts
359 to form as well [26]. It was further shown that a high Sr concentration enhances aragonite
360 precipitation [24,27]. Additionally Roncal-Herrero *et al*. [28] have shown that in the presence of
361 Sr, vaterite can become the dominant carbonate phase even at relatively low temperatures (25°C)
362 .
363 The ~3500 μm thick carbonated front leads to the reduced leachability of the Sr ions, compared to
364 the untreated sample. One possible mechanism for the reduction in ion leachability is porosity
365 clogging which is characteristic to carbonated samples [29,30] as indicated by the densification of
366 the carbonated zone observed in this study (Fig 15). Furthermore, it was shown that vaterite, which
367 was found here as the dominant carbonate phase for these samples, has the lowest density among
368 these carbonate polymorphs, and therefore could lead to increased pore clogging [31].

An additional process that can lead to reduced leachability of Sr is the co-precipitation of Sr into carbonate phases. Aragonite and vaterite have high coordination lattice sites for Sr and Ba and can easily accommodate these larger ions [24,32]. The measured partition coefficient values for Sr in aragonite is of the order of 1.1 at 40°C [33].

The effect of Sr co-precipitation in the metastable carbonate phases can be demonstrated by comparing Ca/Sr weight ratios in the cement paste and in the leachate solutions. In the original cement paste the Ca/Sr ratio is approximately 120. However, a much lower value of 30 was obtained for this ratio in the leachate of the reference sample, due to the preferential incorporation of Ca into crystalline phases and the C-S-H phase, whereas the Sr remains largely interstitial and more available to leaching. In the leachate of the carbonated samples the Ca/Sr ratio is ~45, indicating preferred Sr retention compared to the non-carbonated reference sample. This emphasizes the effect of Sr co-precipitation in aragonite and vaterite, increasing the Sr retention in the paste and thus reducing its relative leachability.

Therefore we may conclude that the clogging effect, which is expected to affect equally all ion mobilities and not to change the Ca/Sr ratio, is secondary in this case.

Additional evidence to the increased Sr retention induced by co-precipitation in aragonite and vaterite phases can be observed by the analysis of the solid matrix. The $[Sr]/[Sr]_0$ ratio within an unleached sample is ~1 throughout the sample, with the exception of the outer surface zone where a large scatter in the results was detected (see section 4.4). All the leached samples that were treated under inert conditions as well as the reference sample show a decrease in the $[Sr]/[Sr]_0$ ratio from a value of 1 in the undisturbed zone to a lower value towards the surface. However, in the samples treated under atmospheric conditions a local enrichment in the $[Sr]/[Sr]_0$ ratio is measured within the aragonite/vaterite precipitation zone, where this ratio reaches the range of 1.2 - 1.4 (Fig. 16).

392 The relative enrichment of Ba in the carbonated front may be related to a similar process occurring
393 due to preferred Ba precipitation in aragonite [34].

394 It is suggested that this enrichment has occurred during the initial carbonation process.
395 Vaterite/aragonite precipitation during the treatment has reduced the local Sr concentration in the
396 pore solution, creating a local gradient in Sr concentration and thus yielding a driving force for Sr
397 diffusion from the surrounding areas to the carbonate precipitation zone. Continuous precipitation
398 of Sr and Ba caused the observed relative enrichments, and thus increased the Sr and Ba ions
399 retention within the sample.

400 It is interesting to note that although the sample carbonated in the climatic chamber showed
401 evidence of cracking at an early stage of the treatment (Fig. 5), this cracking did not lead to higher
402 Sr leachability, supporting the suggestion that Sr immobilization is dominated by its enhanced co-
403 precipitation in the carbonated layer.

404 4.3 The calcite surface layer effect

405 In the analyzed unleached sample, the relative concentration of Ca, Sr and Ba at the outer surface
406 layer showed a large scatter with values ranging between 0.6 and 1.4 (Fig. 3). We suggest that this
407 phenomenon is related to calcite precipitation during sample handling at atmospheric conditions,
408 creating a very thin (10-100 μm) carbonated layer.

409 Additionally, in all leached samples, either treated or untreated, a calcite layer was detected at the
410 outer surface of the sample with thickness varying between 100-500 μm.

411 Calcite precipitation during leaching is reflected in the leaching curves where a change in the slope
412 develops over the square root of time (Figures 6 & 7). A steeper slope was measured over the first
413 7 days of leaching, whereas a more moderate slope persists over the remaining leaching process.

414 This effect was clearly demonstrated for the samples treated in the climatic chamber which have
415 been polished before treatment and therefore they were lacking the initial calcite layer, making the
416 effect more pronounced. This behavior is typical to the formation of a dense impervious
417 carbonation layer and is consistent with previous results by Andac and Glasser [31]. Various other
418 studies investigating the leaching of Portland cement pastes by hydrogeno-carbonate solutions
419 [35,36] or natural waters containing CO_2 [37,38] have shown the formation of a calcite crust, at or
420 near the paste–leachant interface, which strongly slows down the degradation process.

421 Within the near surface calcite layer significant scatter of the Ca, Sr and Ba concentrations occurs.
422 When observing the chemical composition of this layer in leached samples under all treatments,
423 Ca and Sr usually show a reduction in their relative concentration, whereas Ba shows a significant
424 increase in its relative concentration (Figures 10,13&16)

425 The reason for this different behavior is related to the two simultaneous processes of leaching and
426 calcite precipitation. Ca, as a major element, is effectively leached from the sample. Due to its
427 high concentration in the matrix, the small amount of calcite precipitated does not affect the overall
428 trend of the reduction in the Ca relative concentration.

429 On the other hand, Ba, being a trace element is significantly affected from minor precipitation
430 processes. The relatively high Ba enrichment with respect to Sr is mainly the outcome of its lower
431 concentration in the paste and hence higher sensitivity to precipitation processes. This
432 phenomenon is widely used in geological studies, where trace elements are used to emphasize the
433 precipitation of crystalline phases [39].

434 Moreover, the magnitude of this scatter for all three elements is much smaller for the samples
435 treated in the climatic chamber (Fig. 13a) compared with the irradiated samples (Fig. 13b). This is

probably the consequence of the presence of the pre-leaching calcite layer in the later increasing the relative amount of calcite in the sample surface and therefore leading to higher scatter in the element concentrations.

5. Conclusions

The use of local chemical analysis (LA-ICP-MS) together with crystallographic analysis (XRD), supplemented by EPMA imaging, enabled us to link between the crystallography, texture and the composition of the treated samples and their ability to retain Sr ions in the system.

The cementation process is used for the conditioning of low and intermediate level radioactive waste; hence, the effects of irradiation and carbonation are intrinsic to the assessment of the process. However, in the present study no evidence of enhanced degradation mechanisms due to irradiation was found. Carbonation on the other hand, had shown a positive effect on the retention of Sr ions in the matrix with the formation of a distinct carbonated zone at the surface.

In the present study carbonation occurred in three different manners. 1) A very thin (up to 100 μm) carbonated zone was formed during sample preparation and handling. This thin calcite layer was removed for the samples treated in the climatic chamber, leading to an increased Sr leachability compared to samples which were not polished before treatment. 2) All samples exhibited some carbonation (100-500 μm) during the leaching test, performed according to the ANSI-16.1 procedure with no precaution taken to avoid exposure to the atmosphere. 3) For all samples exposed to enhanced carbonation at 40°C, a 3500 μm thick carbonated layer, composed of metastable calcium carbonates (aragonite and vaterite) was formed. These carbonate phases

456 possess high coordination lattice sites for Sr (and Ba) and therefore can easily accommodate these
457 larger ions [32,24].

458 The crystallographic and chemical composition of the samples as well as the retention of Sr ions
459 (representing the immobilized waste) was highly influenced by the latter carbonation process. The
460 extent of carbonation, as well as the crystallography and the Sr retention were similar for both
461 carbonated samples with no additional effect found for the irradiated sample. Thus, carbonation
462 enhanced by temperature increase, is sufficient to explain the retention behavior of strontium under
463 the present atmospheric conditions. The correlation found between relative Sr enrichment and the
464 presence of Ca-carbonate phases, clearly leads to the conclusion that during the carbonation
465 treatment Sr ions are preferentially fractionated into these metastable carbonate phases, leading to
466 a higher retention in the cement paste.

467 References

468 [1] C. Gallé, H. Peycelon, P. Le Bescop, S. Bejaoui, V. L'Hostis, B. Bary, P. Bouniol, C. Richet,
469 Concrete long term behavior in the context of nuclear waste management: Experimental and
470 modeling research strategy, Journal of Physics IV – Proceedings. 136 (2006) 25-38.

471 [2] G. Bar-Nes, A. Katz, Y. Peled, Y. Zeiri, The combined effect of radiation and carbonation on
472 the immobilization of Sr and Cs ions in cementitious pastes, Materials and Structures 41, (2008)
473 1563-1570.

474 [3] F. Vodák, V. Vydra, K. Trtik, O. Kapickova, Effect of gamma irradiation on properties of
475 hardened cement paste, Materials and Structures. 44 (2011) 101-107.

476 [4] V.G. Papadakis, C.G. Vayenas, M.G. Fardis, Fundamental modeling and experimental
477 investigation of concrete carbonation, ACI Materials Journal. 88(4) (1991) 363-373.

478 [5] H. Hyvert, A. Sellier, F. Duprat, P. Rougeau, P. Francisco, Dependency of C–S–H
479 carbonation rate on CO2 pressure to explain transition from accelerated tests to natural
480 carbonation, Cement and Concrete Research. 40, (2010) 1582-1589.

481 [6] M. Castellote, L. Fernandez, C. Andrade, C.Alonso C., Chemical changes and phase analysis
482 of OPC pastes carbonated at different CO2 concentrations, Materials and Structures. 42 (2009)
483 515-525.

484 [7] G.J. Verbeck 1958 Carbonation of hydrated Portland cement, Am Soc Test Mater. 205,
485 (1958) 17-36.

486 [8] H. Wierig, Longtime studies on the carbonation of concrete under normal outdoor exposure,
487 Proc. of RILEM seminar on the durability of concrete structures under normal outdoor exposure,
488 Hannover, Germany, (1984) 239-249.

489 [9] I. Galan, C. Andrade, M. Castellote, Natural and accelerated CO2 binding kinetics in cement
490 paste at different relative humidities, Cement and Concrete Research. 49 (2013) 21-28.

491 [10] Mori et al. 1972 On carbonation of Portland blast-furnace slag cement concrete,
492 Proceedings of the 26th general meeting of the Cement Association of Japan, Tokyo, 184-188.

493 [11] T. Uomoto, Y. Takada, Factors affecting concrete carbonation ratio, Concrete Library of
494 JSCE 21, (1993) 31-44.

[12] E. Drouet, S. Poyet, P. Le Bescop, J.M. Torrenti, J M, Chemical changes and carbonation profiles of carbonated cement pastes at 80°C for different relative humidities, Proceedings of CONSEC'10, 2010, Merida, Mexico.

[13] A.C. Garrabrants, F. Sanchez, D.S. Kosson, Changes in constituent equilibrium leaching and pore water characteristics of a Portland cement mortar as a result of carbonation, Waste Management, 24(1) (2004) 19–36.

[14] J.C. Walton, M.S.Bin Shafique, R.W. Smith, N. Gutierrez, A.J. Tarquin, Role of carbonation in transient leaching of cementitious wasteforms, Environmental Science and Technology. 31 (1997) 2345-2349.

[15] T. Van Gerven, D. Van Baelen, V. Dutre, C. Van de casteele, Influence of carbonation and carbonation methods on leaching of metals from mortars, Cement and Concrete Research. 34 (2004) 149–156.

[16] M.S. Bin Shafique, J.C. Walton, N. Gutierrez, R.W. Smith, A.J. Tarquin, Influence of carbonation on leaching of cementitious wasteforms, Journal of Environmental Engineering (ASCE). 124 (1998) 463–467.

[17] P.H.R. Borges, J.O. Costa, N.B. Milestone, C.J. Lynsdale, R.E. Streatfield, Carbonation of CH and C–S–H in composite cement pastes containing high amounts of BFS, Cement and Concrete Research. 40 (2013) 284-292.

513 [18] J. Han, W. Sun, G. Pan, W. Caihui, Monitoring the evolution of accelerated carbonation of
514 hardened cement pastes by x-ray computed tomography, Journal of Materials in Civil Engineering.
515 25 (2013) 347-354.

516 [19] M. Auroy, S. Poyet, P. Le Bescop, J.M. Torrenti, T. Charpentier, M. Moskura, X. Bourbon,
517 Impact of carbonation on unsaturated water transport properties of cement-based materials,
518 Cement and Concrete Research. 74 (2015) 44-58.

519 [20] L. Greenspan, Humidity fixed points of binary saturated aqueous solutions, Journal of
520 Research of the National Bureau of Standards – A. Physics and Chemistry. 81A (1977) 89-96.

521 [21] Q. Johnson, R.S. Zhou, Checking and estimating RIR values, JCPDS-International Centre
522 for Diffraction Data, Advances in X-ray Analysis. 42 (2000) 287-296.

523 [22] ANSI/ANS-16.1–1986 (1986) Measurement of the leachability of solidified low-level
524 radioactive wastes by a short term test procedure. American Nuclear Society, IL, USA

525 [23] T. Ogino, T. Suzuki, K. Sawada, The formation and transformation mechanism of calcium
526 carbonate in water, Geochimica and Cosmochimica Acta. 51(10) (1987) 2757-2767.

527 [24] J.L. Wray, F. Daniels, Precipitation of Calcite and Aragonite, Journal of the American
528 Chemical Society. 79(7) (1957) 2031-2034.

529 [25] M.L.D. Gougar, B.E. Scheetz, D.M. Roy, Ettringite and C-S-H Portland Cement Phases for
530 Waste Ion Immobilization: A Review. Waste Management. 16(4) (1996) 295-303.

[26] E.T. Stepkowska, J.L. Pérez-Rodríguez, M.J. Sayagués, J.M. Martínez-Blanes, Calcite, Vaterite and Aragonite forming on cement hydration from liquid and gaseous phase, Journal of Thermal Analysis and Calorimetry. 73 (2003) 247-269.

[27] I. Sunagawa, Y. Takahashi, H. Imai, Strontium and aragonite-calcite precipitation, J. mineralogical and petrological sciences. 102 (2007) 174-181.

[28] T. Roncal-Herrero, J.D. Rodriguez-Blanco, P. Bots, S. Shaw, L.G. Benning, The Role of Zn, Sr, Mg and PO4 in the Interaction of Carbonate-Rich Waters with Sulphate Minerals, revista de la sociedad española de mineralogía. 15 (2011) 181.

[29] V.T. Ngala, C.L. Page, Effects of carbonation on pore structure and diffusional properties of hydrated cement pastes, Cement and Concrete research. 27(7) (1997) 995-1007.

[30] P. A. Claisse, H. El-Sayad, I.G. Shaaban, Permeability and pore volume of carbonated concrete, ACI Materials Journal. 96 (3) (1999) 378-382.

[31] M. Andac & F.P. Glasser, Long-Term leaching mechanisms of Portland cement-stabilized municipal solid waste fly ash in carbonated water, Cement and Concrete Research. 29 (1999) 179-186.

[32] J.L. Banner, Application of the trace element and isotope geochemistry of strontium to studies of carbonate diagenesis, Sedimentology. 42 (1995) 805-824.

[33] D.J.J. Kinsman, H.D. Holland, The co-precipitation of cations with CaCO3-IV. The co-precipitation of Sr^{+2} with aragonite between 16° and 96°C, Geochim. Cosmochim. Acta. 33 (1969) 1–17.

551 [34] M. Dietzel, N. Gussone, A. Eisenhauer, Co-precipitation of Sr^{2+} and Ba^{2+} with aragonite by
552 membrane diffusion of CO2 between 10 and 50°C, Chemical geology. 203 (2004) 139-151.

553 [35] Badouix et al. 1999 Toward a validation of the modeling of concrete long term alteration by
554 natural water attack. Global proceedings

555 [36] I. Kurashige, M. Hironaga, K. Niwase, Effects of hydrogencarbonate and chloride in ground
556 water on leaching of cementitious materials. CONSEC'07 Tours, (2007) 615-622.

557 [37] J. Cowie, F.P. Glasser, The reaction between cement and natural waters containing
558 dissolved carbon dioxide, Advanced in Cement Research. 4 (1992) 119-134.

559 [38] A. Dauzères, P. Le Bescop, P. Sardini, C. Cau Dit Coumes, Study of CEMI and low pH
560 cement pastes leaching in multi-ionic underground water. CONSEC'10 Mérida, (2010) 495-503

561 [39] Winter J.D., An introduction to igneous and metamorphic petrology, 2001, Prentice Hall.

562

563 Funding: This work was supported by the Israel Atomic Energy Commission (IAEC) and the
564 French Alternative Energies and Atomic Energy Commission (CEA).

565

566

567

568

569 Table 1: Chemical composition of CEM I Val d'Azergues cement (wt%) (Producers data)

SiO_2	Al_2O_3	Fe_2O_3	CaO	MgO	K_2O	Na_2O	SO_3	S^{-2}	Cl^-	P_2O_5	LOI
20.6	3.6	5.0	64.3	0.7	0.7	0.2	2.7	0.01	0.06	0.4	1.1

570

571

572

573

574

575

576

577

578

579

580

581

582

583

584 Table 2: List of samples (irradiation=IR, climatic chamber=CC, atmospheric=At, inert=In)

Sample experimental condition	Sr doping	Polished before treatment	Treatment	External conditions	leaching	comments
Reference	+	-	-	_	+	
Climatic chamber atmospheric	+	+	CC	At	+	
Climatic chamber inert	+	+	CC	In	+	
Irradiated atmospheric	+	-	IR	At	+	
Irradiated inert (blank)	_	-	IR	In	+	Natural Sr concentration
Irradiated inert (unleached)	+	-	IR	In	-	

585

586

587

588

589

590

591

592 Table 3: Crystallographic data for the XRD RIR analysis (from ICSD using POWD-12++)

mineral	2θ	RIR	peak fraction
Calcite	29.3	3.2	1
Aragonite	26.1	1.13	1
Vaterite	26.9	1.14	1
Portlandite	17.9	3.46	0.74

593

594

595

596

597

598

599

600

601

602

603

604 Table 4: List of analyzed isotopes, their average limit of detection and average analytical error
605 percent for the different spot sizes

606

Spot size	10 μm		50 μm		100 μm	
	LOD (μg/g)	% error	LOD (μg/g)	% error	LOD (μg/g)	% error
^{25}Mg	76	2.4	2.7	0.6	0.9	0.2
^{29}Si	3083	1.7	111	0.4	29	0.1
^{42}Ca	3696	1.0	94	0.1	26	0.1
^{43}Ca	1653	1.5	68	0.3	24	0.1
^{88}Sr	1.4	0.8	0.1	0.2	0.02	0.1
^{137}Ba	7.3	8.1	0.4	1.9	0.1	0.8

607

608

609

610

611

612

613

Figure captions:

Figure 1: The sampling spot size and relative concentration of Ca and Mg as a function of the distance from the sample surface in a leached sample. C = the concentration at a specific distance, C_0 = the concentration at the undisturbed inner sample volume.

Figure 2: EPMA BSE image of sample surface irradiated under inert atmosphere.

Figure 3: Relative concentration of Ca, Ba and Sr as obtained by LA-ICPMS along a cross section in a sample irradiated under inert conditions

Figure 4: XRD profiles of samples treated under atmospheric conditions. (a) sample treated in climatic chamber, (b) sample irradiated

Figure 5: Cracking on sample exposed to atmospheric conditions in the climatic chamber

Figure 6: Sr Cumulative fraction as a function of square root of leaching time. The error bars represent the average deviation of duplicate samples.

Figure 7: Ca Cumulative fraction as a function of square root of leaching time. The error bars represent the average deviation of duplicate samples

Figure 8: Sr Cumulative fraction for samples irradiated under inert conditions doped and un-doped with Sr as a function of square root of leaching time.

Figure 9: EPMA BSE image of the untreated reference leached sample

Figure 10: the Sr, Ca and Ba concentration variation along a cross section in the untreated reference leached sample

Figure 11: XRD profile of the untreated reference leached sample

Figure 12: EPMA BSC image of leached sample after treatment in the climatic chamber under inert atmosphere.

Figure 13: LA-ICP-MS Ca, Ba and Sr concentration variation along a cross section in the two leached samples after treatment under inert atmosphere.(a) climatic chamber (b) irradiated

Figure 14: Phase distribution along a cross section in the leached samples after treatment under inert atmosphere (a) in the climatic chamber (b) irradiated

Figure 15: EPMA BSE images of leached sample treated in the climatic chamber under atmospheric conditions. Zoom into the near edge area (surface on the top).

Figure 16: The Ca, Ba and Sr concentrations along a cross section in leached samples after treatment under atmospheric conditions; (a) in the climatic chamber (b) irradiated

Figure 17: Phase distribution along a cross section in the leached samples after treatment under atmospheric conditions (a) in the climatic chamber (b) irradiated

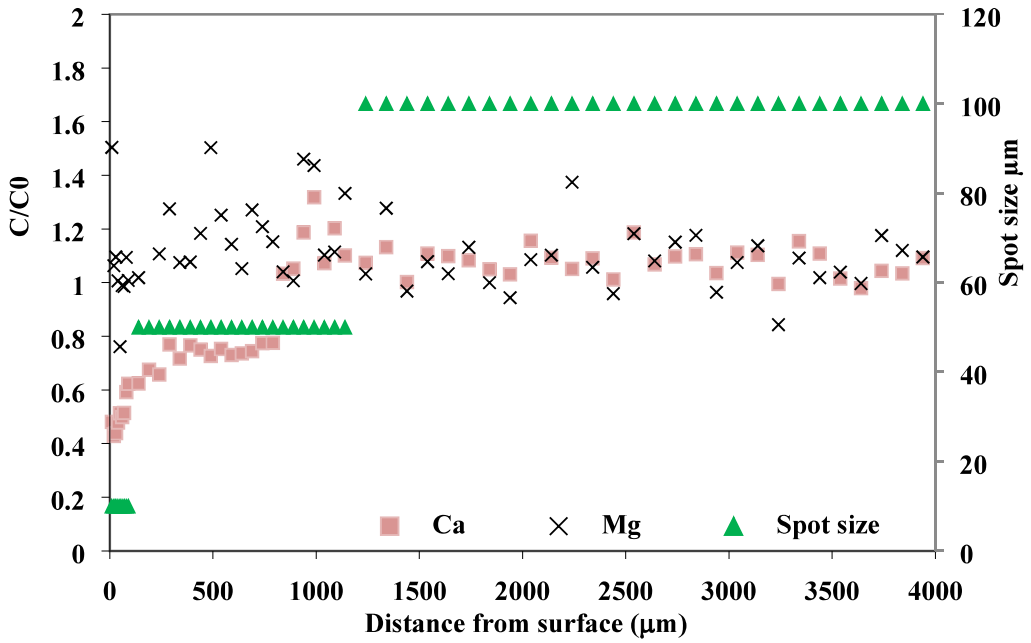

Figure 1: The sampling spot size and relative concentration of Ca and Mg as a function of the distance from the sample surface in a leached sample. C = the concentration at a specific distance, C_0 = the concentration at the undisturbed inner sample volume.

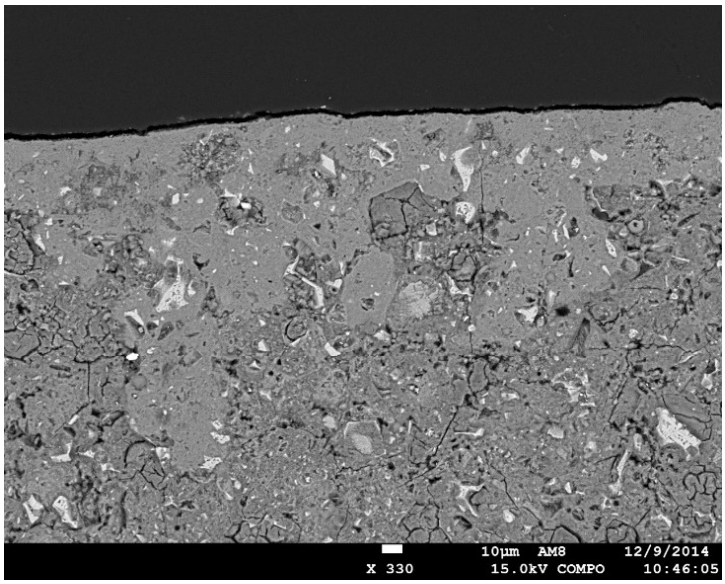

Figure 2: EPMA BSE image of sample surface irradiated under inert atmosphere.

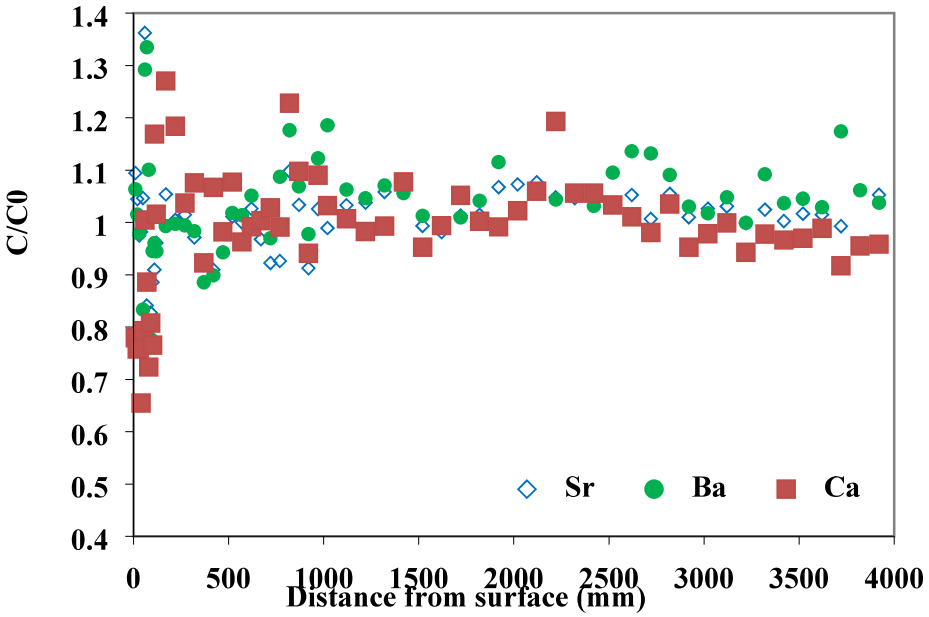

Figure 3: Relative concentration of Ca, Ba and Sr as obtained by LA-ICPMS along a cross section in a sample irradiated under inert conditions

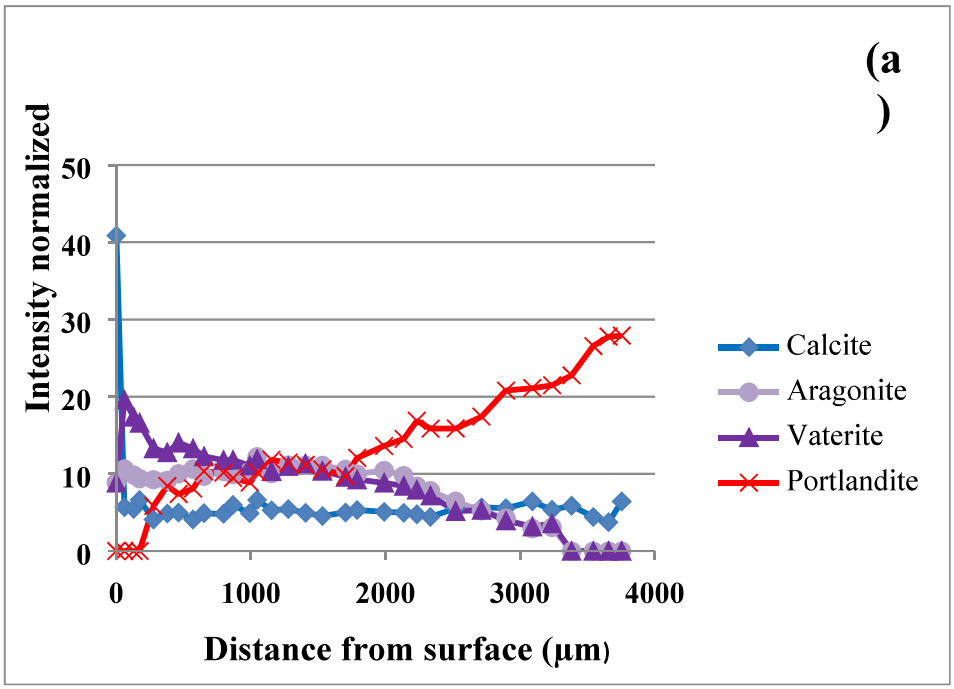

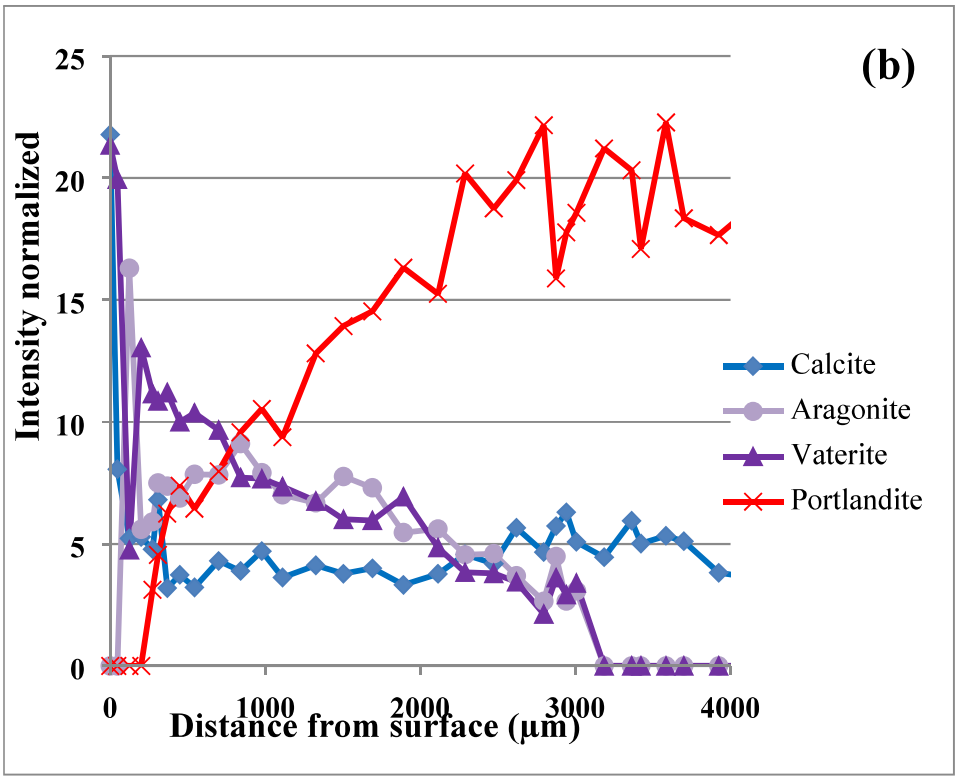

Figure 4: XRD profiles of samples treated under atmospheric conditions. (a) sample treated in climatic chamber, (b) sample irradiated

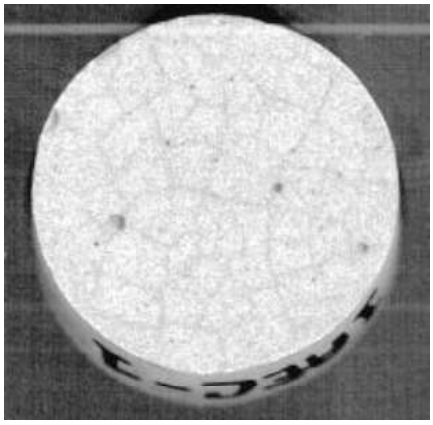

Figure 5: Cracking on sample exposed to atmospheric conditions in the climatic chamber

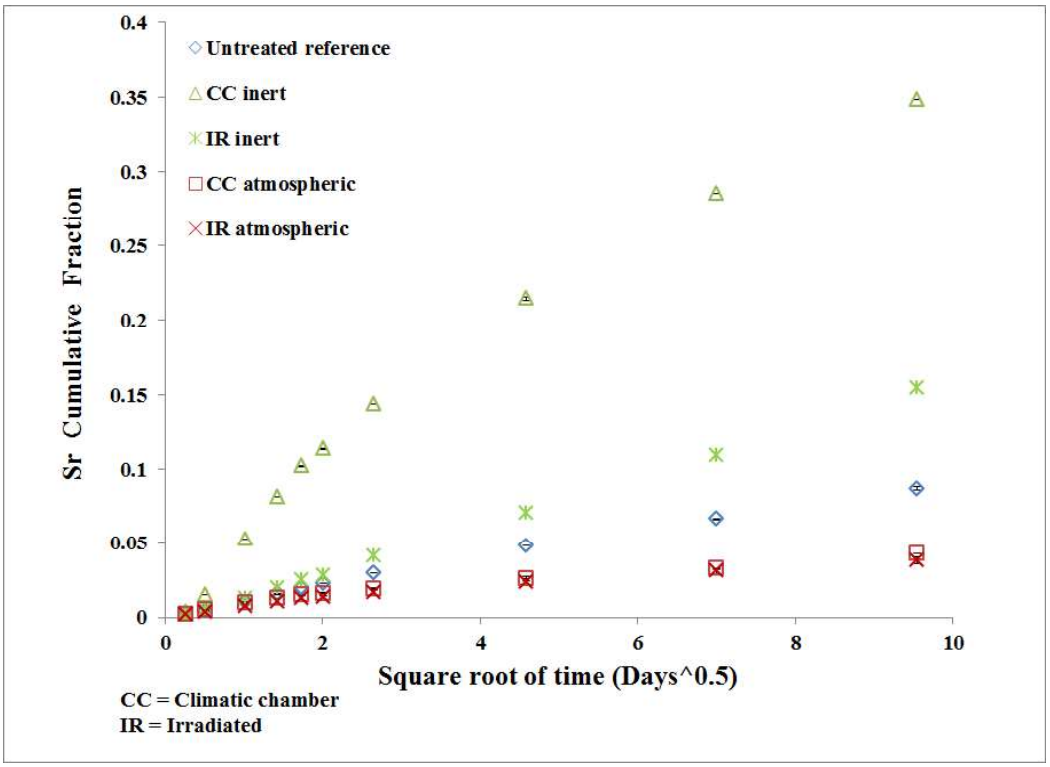

Figure 6: Sr Cumulative fraction as a function of square root of leaching time. The error bars represent the average deviation of duplicate samples.

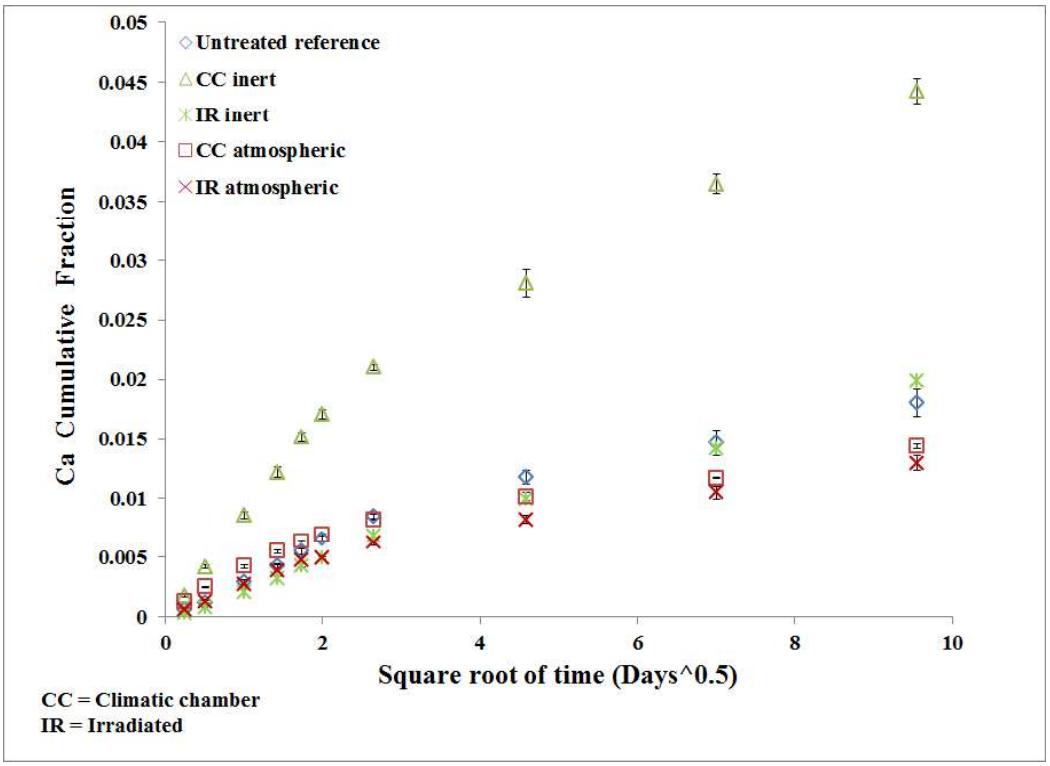

Figure 7: Ca Cumulative fraction as a function of square root of leaching time. The error bars represent the average deviation of duplicate samples

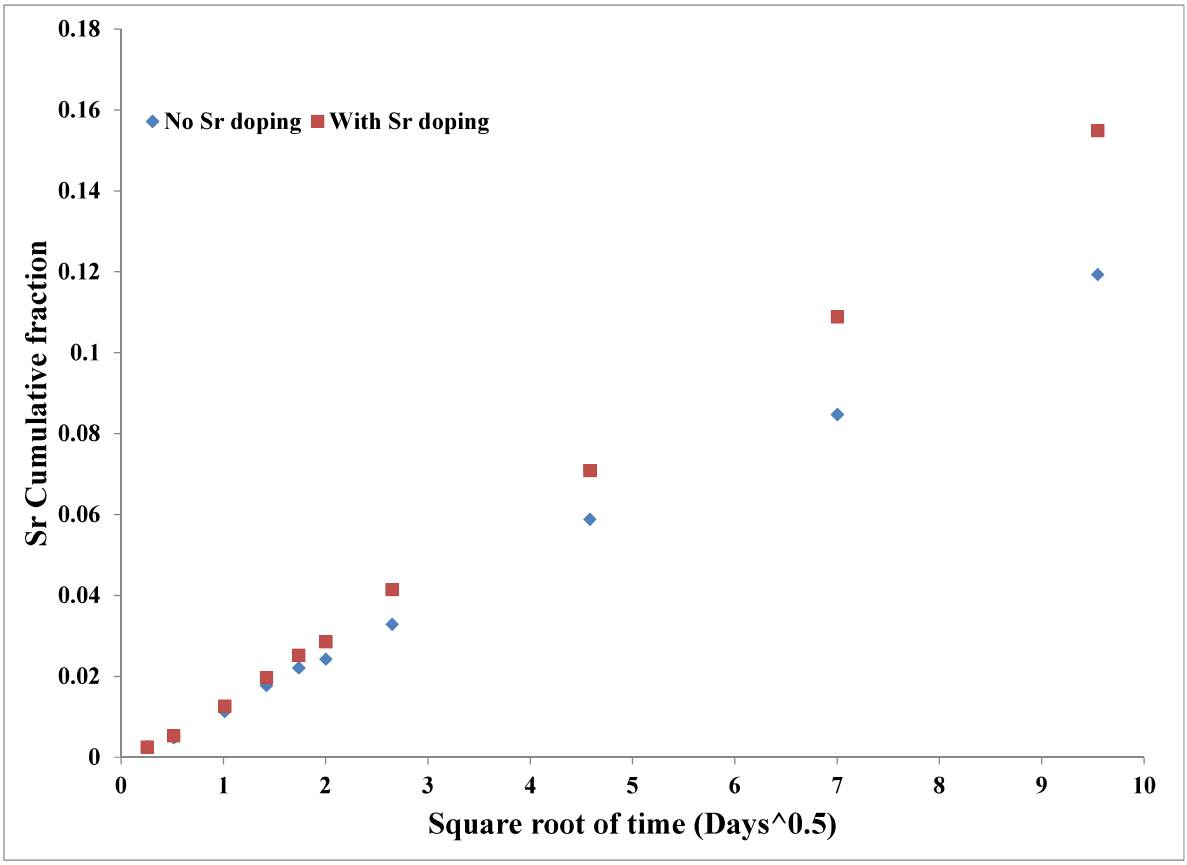

Figure 8: Sr Cumulative fraction for samples irradiated under inert conditions doped and un-doped with Sr as a function of square root of leaching time.

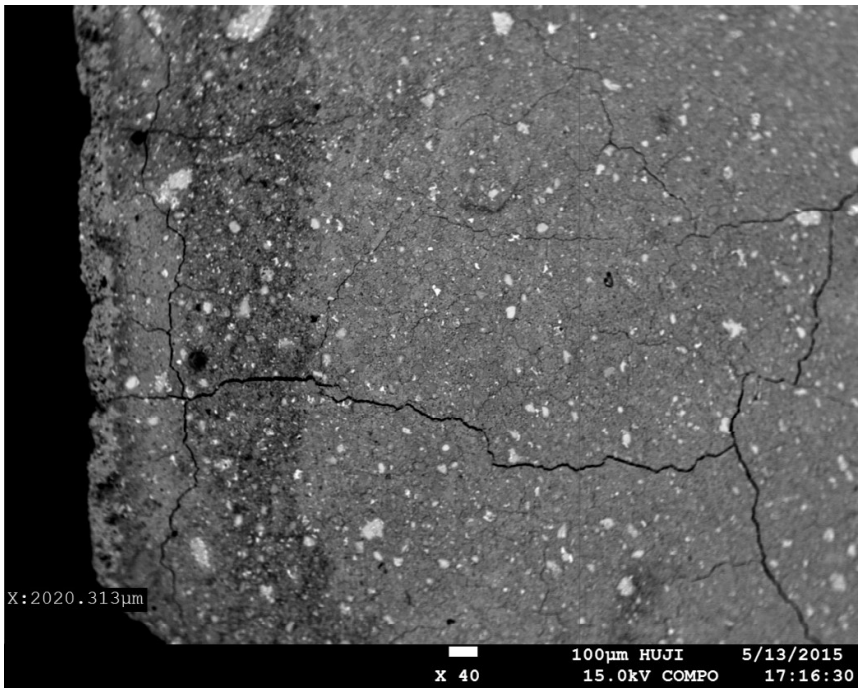

Figure 9: EPMA BSE image of the untreated reference leached sample

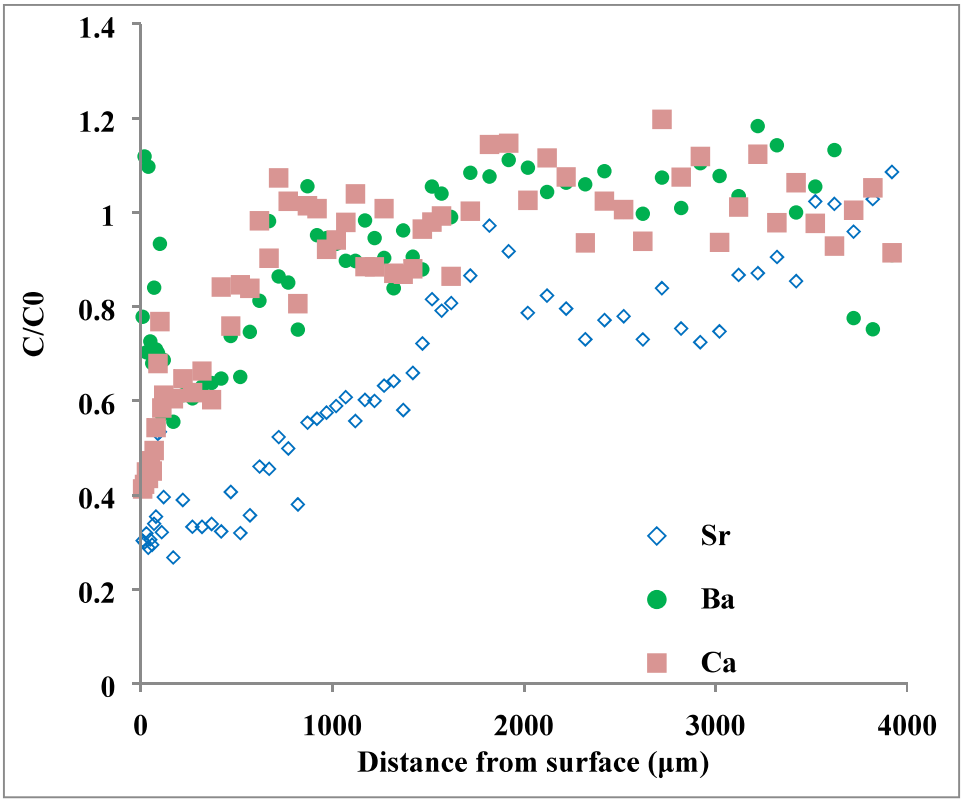

Figure 10: the Sr, Ca and Ba concentration variation along a cross section in the untreated reference leached sample

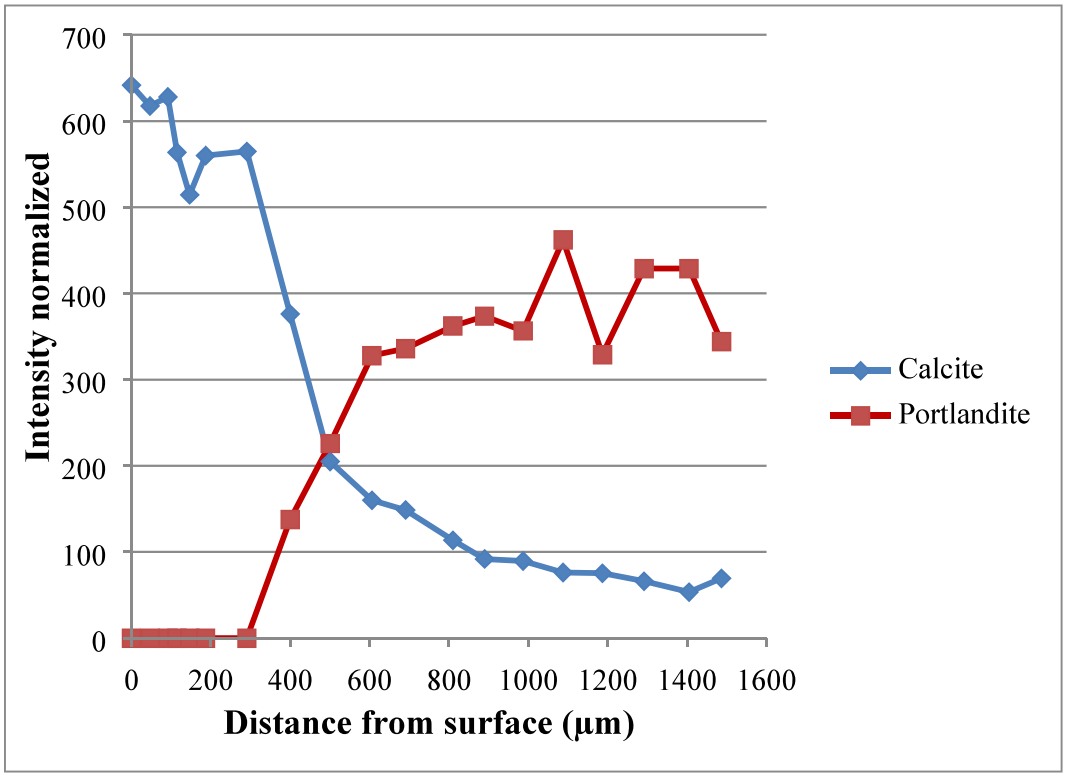

Figure 11: XRD profile of the untreated reference leached sample

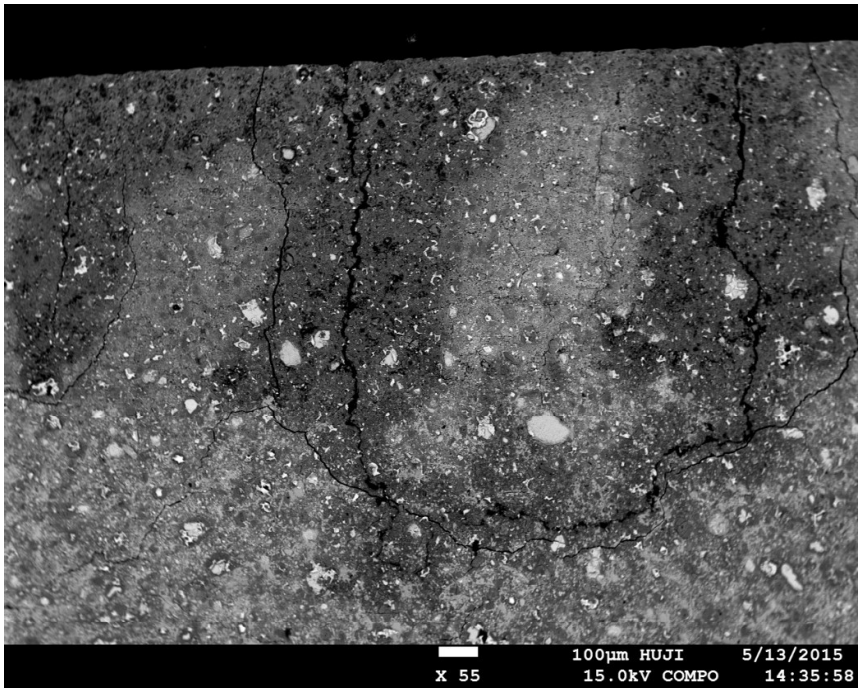

Figure 12: EPMA BSC image of leached sample after treatment in the climatic chamber under inert atmosphere.

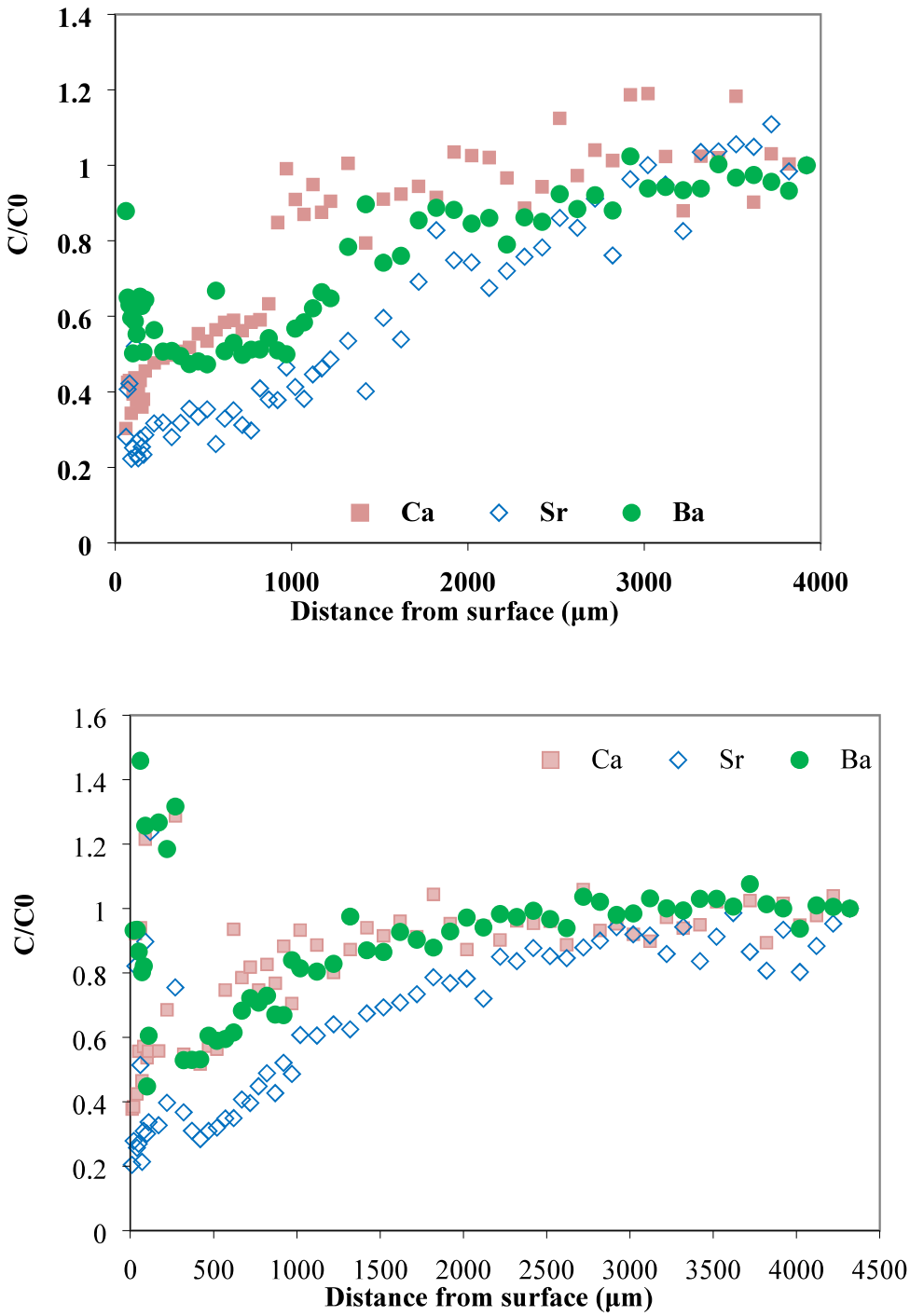

Figure 13: LA-ICP-MS Ca, Ba and Sr concentration variation along a cross section in the two leached samples after treatment under inert atmosphere:(a) climatic chamber (b) irradiated

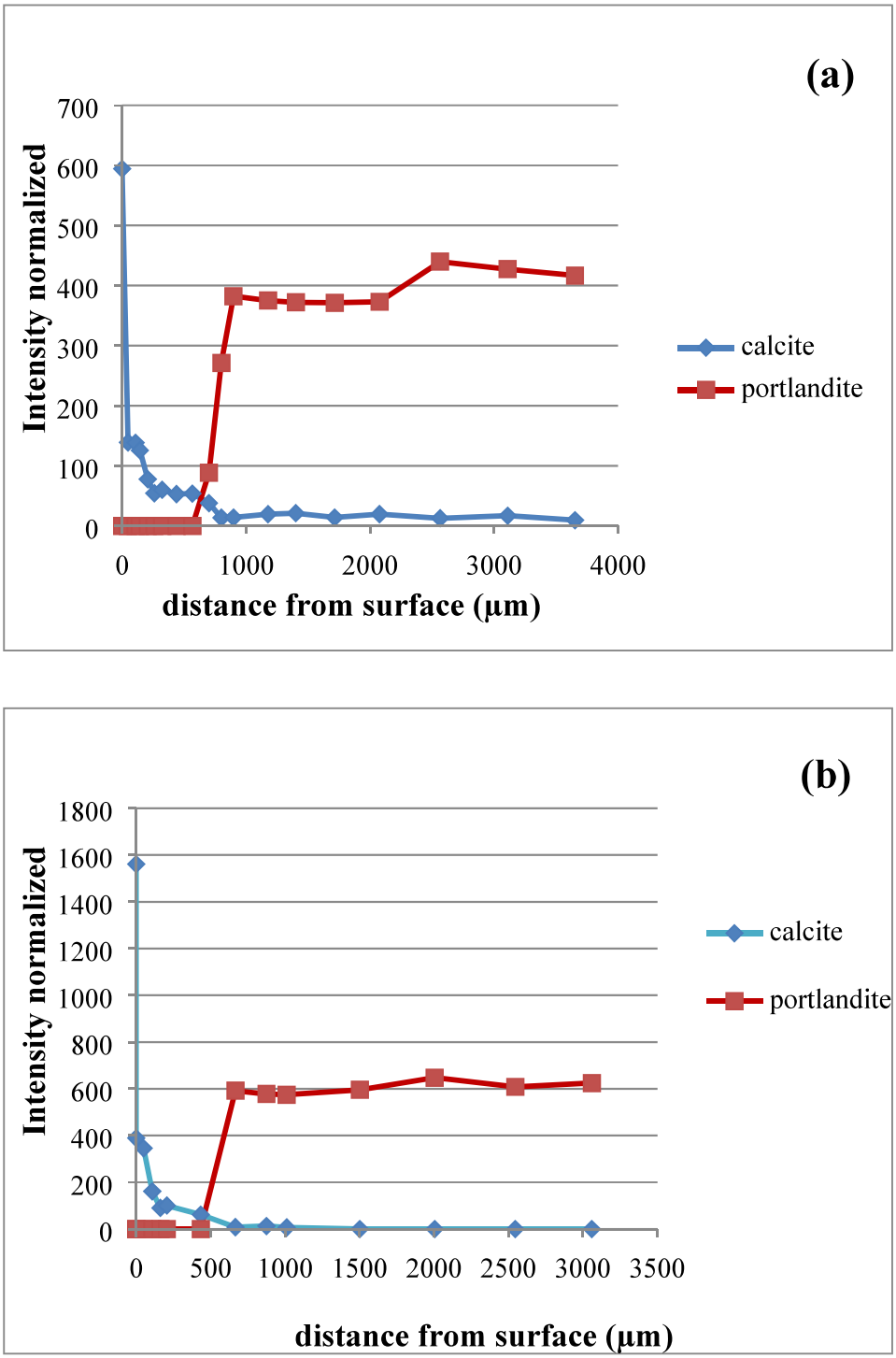

Figure 14: Phase distribution along a cross section in the leached samples after treatment under inert atmosphere (a) in the climatic chamber (b) irradiated

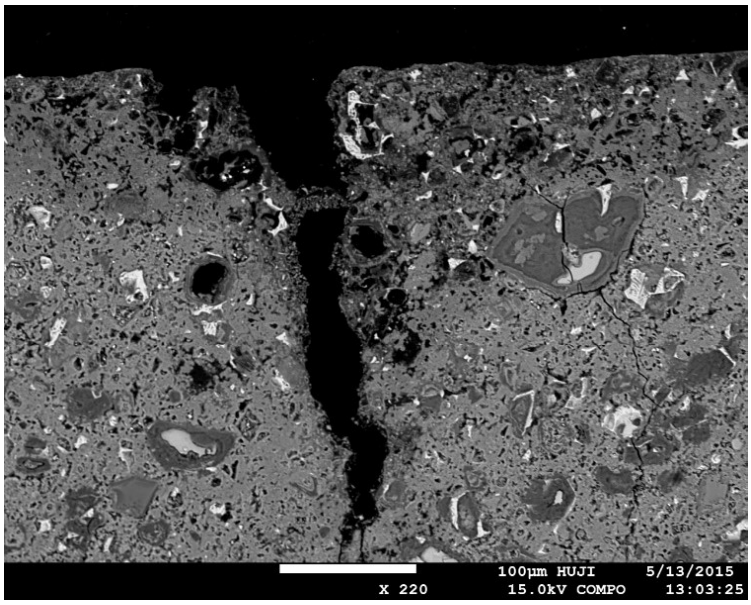

Figure 15: EPMA BSE images of leached sample treated in the climatic chamber under atmospheric conditions. Zoom into the near edge area (surface on the top).

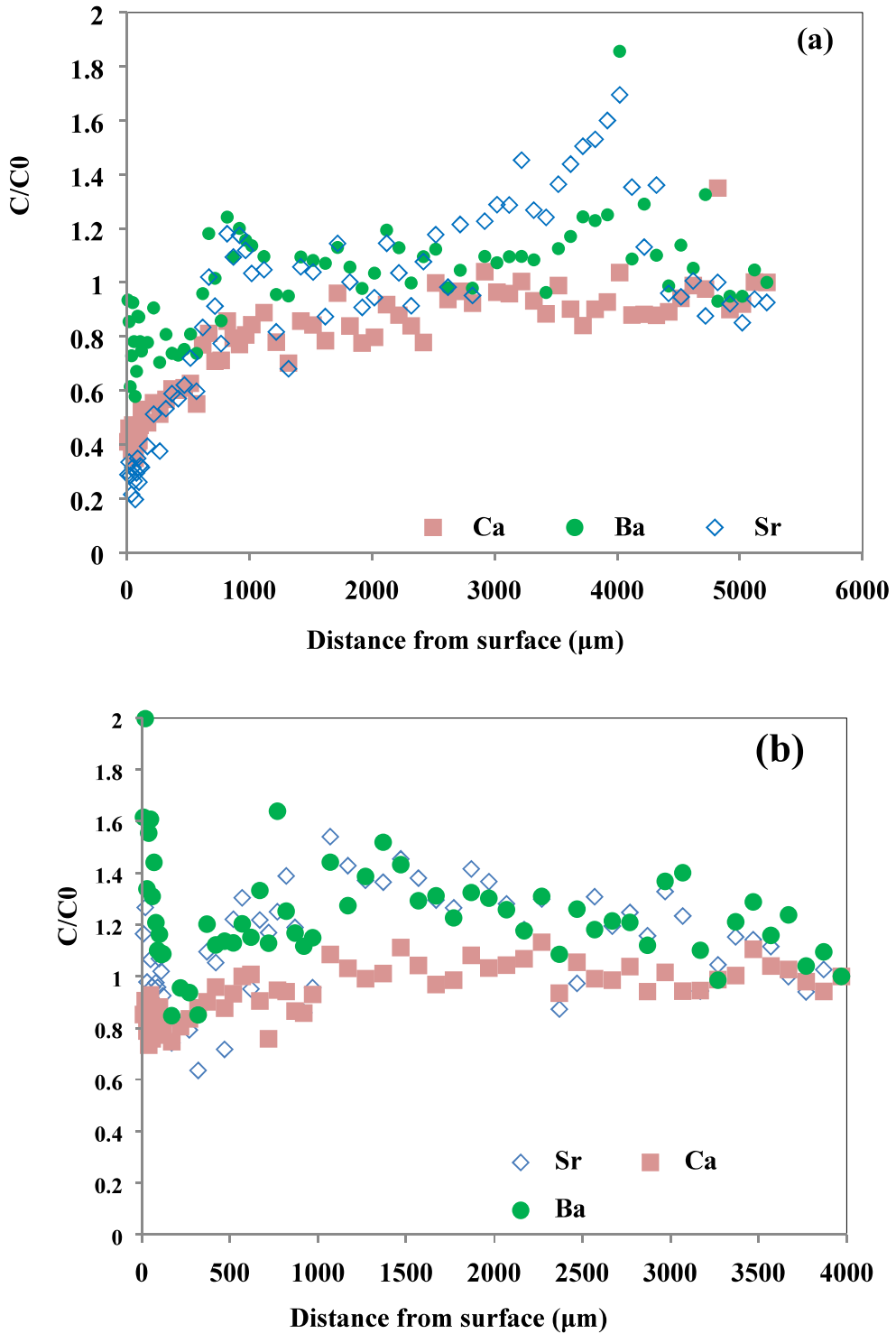

Figure 16: The Ca, Ba and Sr concentrations along a cross section in leached samples after treatment under atmospheric conditions; (a) in the climatic chamber (b) irradiated

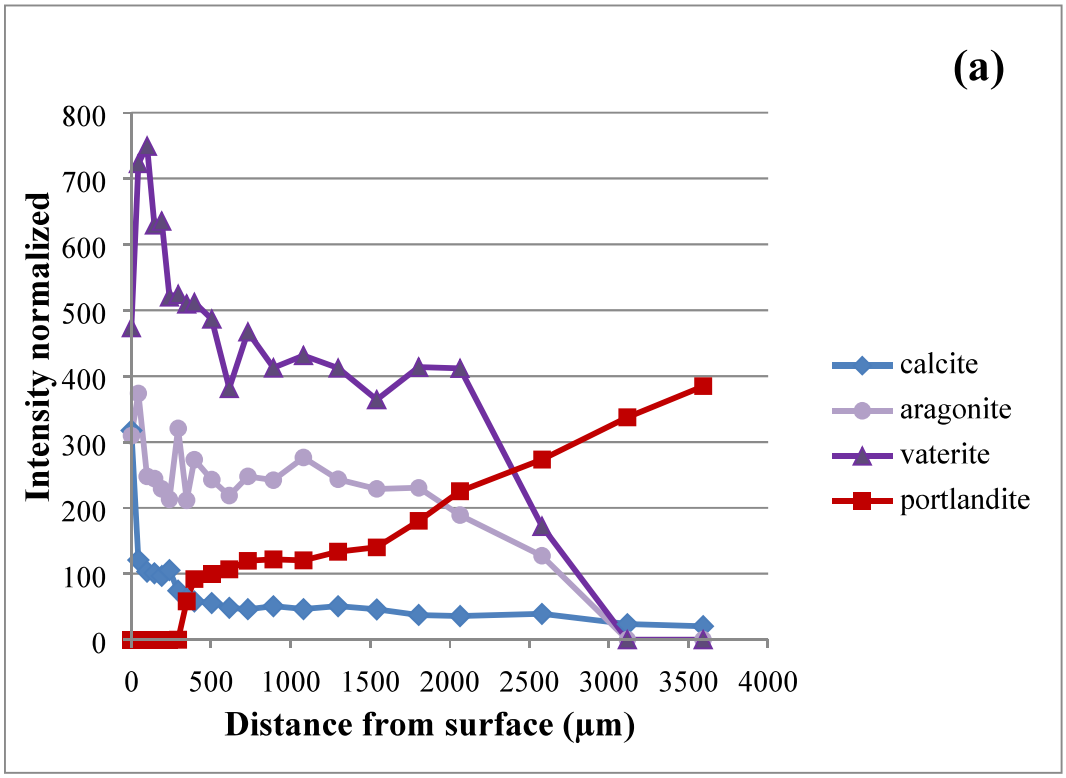
(a)
Intensity normalized
800
700
600
500
400
300
200
100
0
0
500
1000
1500
2000
2500
3000
3500
4000
Distance from surface (µm)
calcite
aragonite
vaterite
portlandite

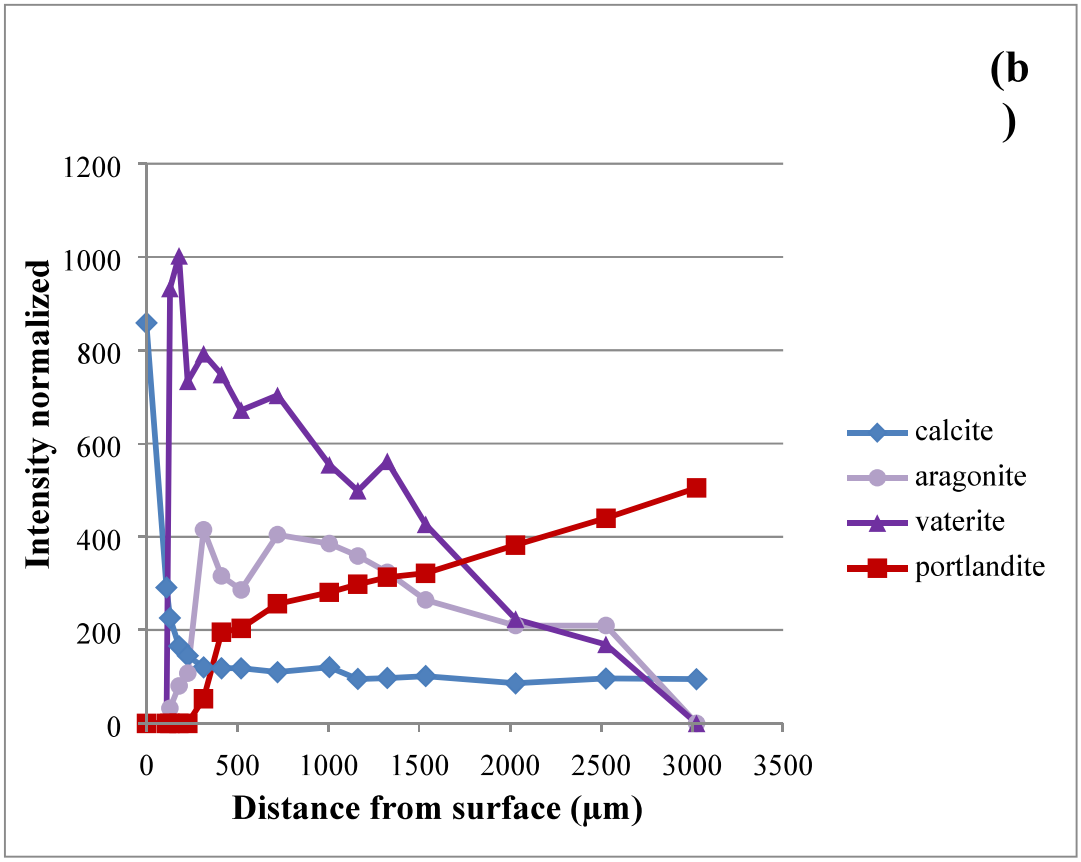
(b
)
Intensity normalized
1200
1000
800
600
400
200
0
0
500
1000
1500
2000
2500
3000
3500
Distance from surface (µm)
calcite
aragonite
vaterite
portlandite

Figure 17: Phase distribution along a cross section in the leached samples after treatment under atmospheric conditions (a) in the climatic chamber (b) irradiated